ACS APPLIED MATERIALS & INTERFACES

Research Article

www.acsami.org

Novel Architecture of Plasmon Excitation Based on Self-Assembled Nanoparticle Arrays for Photovoltaics

Hanggochnuri Jo,[†,§] Ahrum Sohn,[‡,§] Kyung-Sik Shin,[†] Brijesh Kumar,[†] Jae Hyun Kim,[⊥] Dong-Wook Kim,[‡] and Sang-Woo Kim*[,†,∥]

[†]School of Advanced Materials Science and Engineering, Sungkyunkwan University (SKKU), Suwon 440-746, Republic of Korea

[‡]Department of Physics, Ewha Womans University, Seoul 120-750, Republic of Korea

[⊥]Department of Energy Research, Daegu-Gyeongbuk Institute of Science and Technology, Daegu 711-873, Republic of Korea

[∥]SKKU Advanced Institute of Nanotechnology (SAINT), Center for Human Interface Nanotechnology (HINT), Sungkyunkwan University (SKKU), Suwon 440-746, Republic of Korea

ABSTRACT: An efficient approach to producing hexagonally self-assembled and well-dispersed gold (Au) nanoparticles (NPs) in the pores of porous anodic aluminum oxide (AAO) is reported. This approach is particularly useful for tuning the surface plasmon resonance frequency of Au NPs by varying the effective dielectric constant of AAO. A strongly enhanced Raman spectrum of dye molecule rhodamine 6G using these well-dispersed Au NPs revealed that such a self-assembled Au NP array can induce a strong plasmonic field. Furthermore, we demonstrated a new architecture of plasmon excitation in a bulk heterojunction (BHJ) inverted organic solar cell (IOSC) using the Au NP array with AAO. The optical response of an active layer poly(3-hexylthiophene):(6,6)-phenyl-C_{61}-butyric acid methyl ester was enhanced by this strong plasmonic field associated a well-dispersed Au NP array. A comparative study of AAO with and without Au NPs confirmed plasmonic improvement of the BHJ IOSC. Simulation results showed that Au NPs concentrate the incoming light into a strongly localized field and enhance light absorption in a wide wavelength range.

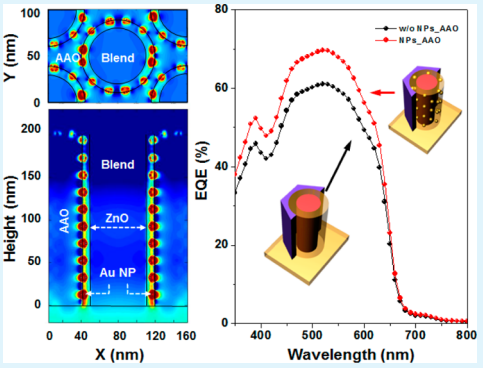

KEYWORDS: *plasmonic effect, AAO template, ZnO, self-assemble, surface-enhanced Raman spectroscopy, organic solar cell*

INTRODUCTION

Noble-metal nanoparticles (NPs) and their optical properties originating from localized surface plasmon resonance (LSPR) have motivated many studies, especially those on their controlled synthesis and photonic applications.[1−7] LSPR is the collective oscillation of the free electrons in a metal, which occurs when the incoming light wave meets the resonance conditions.[6,7] At resonance, a highly localized field is formed at a NP, which greatly enhances absorption. LSPR also dramatically increases the far-field scattering cross section of a NP. LSPR modes depend on the geometric properties and dielectric function of NPs and their surrounding medium.[8−11] A metal NP array exhibits unique electronic and magnetic properties, especially depending on the precise control of the NP shape and size and the interparticle spacing.[12,13] These properties, which are related to LSPR, can become more pronounced when the NPs are periodically arranged.[14] In addition, the dielectric surroundings of these NPs influence the coherent excitation of electronic density oscillations and the associated LSPR modes, which results in modification of the enhanced field strength and optical spectral response.[13,14]

The size, shape, and interparticle distance of metal NPs must be controlled precisely to obtain desirable plasmonic effects. Top-down approaches, such as e-beam lithography and focus-ion-beam milling, are excellent for controlling the above-mentioned parameters, but their high cost and poor throughput limit their use in sample fabrication. Instead, solution-phase colloidal NPs have been widely used as plasmonic nanostructures.[15−18] However, colloidal aggregations and hot spots in dispersed nanoscale systems are randomly distributed.[19] Thus, it is very desirable to fabricate a reproducible and uniform plasmonic NP array, where hot spots are regularly distributed. One promising approach is to realize a uniform array of plasmonic metal NPs via a porous anodic aluminum oxide (AAO) template.[20,21] AAO templates can be used to directly produce a plasmonic nanoarray.[22]

In this work, we report well-dispersed Au NPs on the hexagonally structured pores of an AAO template. The AAO template approach is an easy and efficient method for realizing well-dispersed metallic nanostructures, providing control over the particle size and density. The plasmon frequency can be tuned by varying the effective dielectric constant of AAO using hexagonally well-dispersed Au NPs. Surface-enhanced Raman spectroscopy (SERS) revealed that such a self-assembled Au

Received: October 16, 2013
Accepted: December 16, 2013
Published: December 16, 2013

   dx.doi.org/10.1021/am4045585 | ACS Appl. Mater. Interfaces 2014, 6, 1030−1035

NP array can induce a very strong plasmonic field. Furthermore, by using the Au NP array with AAO, we propose a new architecture of plasmon excitation in a bulk heterojunction (BHJ) inverted organic solar cell (IOSC) to enhance the plasmon effect. A comparative study of AAO with and without Au NPs clearly showed the LSPR effects on the optical and current density−voltage (J−V) characteristics of the BHJ IOSC. Numerical simulations confirmed the plasmonic improvement of this new BHJ solar cell.

EXPERIMENTAL SECTION

Preparation of the AAO Template with Au NPs. AAO templates with hexagonally arrayed nanopores are typically fabricated by two-step anodization of aluminum (Al). A pure Al sheet (99.999%) of thickness 0.5 mm was electropolished in a mixture of perchloric acid and ethanol ($HClO_4$:C_2H_5OH = 1:4 volumetric ratio) at a constant voltage of 20 V and a temperature of 7 °C to remove surface irregularities. Next, a 0.3 M oxalic acid solution was used to fabricate AAO structures having an initial pore diameter of 30 nm and a periodic pore-to-pore distance of 100 nm for 12 h at 40 V and 15 °C (first anodization) without the use of a widening process. Then, the AAO layer was removed in a mixture of 1.8 wt % chromic acid and 6 wt % phosphoric acid for 6 h at 65 °C. Highly ordered AAO templates were obtained by a second anodization under the same conditions as those in the first anodization. The AAO depth was determined from the duration of the second anodization. To increase the AAO pore size, the AAO templates were etched in 0.1 M phosphoric acid at 30 °C. A 10-nm-thick Au thin film was deposited on AAO at an evaporation rate of 2 Å using a thermal evaporation technique and then thermally annealed at 600 °C for 1 h under atmosphere to prepare the Au NP arrays.[23]

Fabrication of a Photovoltaic Device. To fabricate the IOSCs with the AAO template,[24] we transferred AAO with and without Au NPs on the substrates. First, commercial indium−tin oxide (ITO)-coated glass substrates were used to deposit the 50-nm-thick film using zinc oxide (ZnO) sol, and then AAO templates with/without Au NPs were transferred onto these ZnO-deposited substrates. ZnO nanotubes inside the AAO template were made by spin coating of ZnO sol at 300 rpm. For infiltration of ZnO sol into the AAO pore, the AAO template was placed in a vacuum chamber for 10 min and then dried at 150 °C outside of the chamber for 30 min. Polymer blend poly(3-hexylthiophene):(6,6)-phenyl-C_{61}-butyric acid methyl ester (P3HT:PCBM) was spin-coated at 500 rpm for 30 s into ZnO nanotubes made in the pores of AAO with and without Au NPs. Then, the samples were kept in a covered glass Petri dish for solvent annealing. Annealing was performed at 110 °C for 10 min. Molybdenum oxide (MoO_3) as an electron blocking layer and a silver (Ag) anode were subsequently deposited via thermal evaporation. The IOCSs with/without Au NPs were fabricated in parallel.

Characterization. UV−vis photospectrometry was used to measure the reflectance of the samples. SERS spectra were measured by a Raman system (Renishaw, RM1000-Invia) with an excitation wavelength of 633 nm, where the effective power of the laser source was 30 W and the integration time was 10 s. To describe the electromagnetic field distribution in the samples, Maxwell equations were solved by the finite-difference time-domain (FDTD) method. The repeated structure with the AAO template was modeled in FDTD (Lumerical FDTD Solutions). In the unit cell, the Au NPs with diameter of 10 nm were put on the side walls with a separation of 20 nm between the nearest neighbors. Such size and distance were chosen to be the values observed in the field-emission scanning electron microscopy (FE-SEM) measurements. The polarization and propagation directions of the incident plane waves were parallel to the surface and pore axes of the AAO template, respectively. Perfectly matched layer boundary conditions, which absorb incident radiation, were used at the top and bottom faces of the unit cell to avoid nonmeaningful reflection from the simulation boundaries. Periodic boundary conditions were used for the side walls of the unit cell.

RESULTS AND DISCUSSION

We synthesized a self-assembled hexagonally well-dispersed Au NP array with AAO to realize a new architecture of plasmon excitation in BHJ IOSCs and to enhance the plasmon effect. Parts a and b of Figure 1 show FE-SEM images of the AAO template and self-assembled hexagonally well-dispersed Au NPs on the surface and in the pores of AAO, respectively. Figure 1a shows a highly ordered nanoporous array with a uniform pore diameter of 80 nm and a height of 250 nm. Figure 1b reveals the formation of Au NPs on the surface and in the pores of AAO. Figure 1c shows the cross-sectional FE-SEM image of self-assembled well-dispersed Au NPs into the walls of the highly ordered pores of the AAO template, which was transferred onto a ZnO/ITO/glass substrate to fabricate the BHJ IOSCs. The self-assembled well-dispersed Au NPs in the walls of the highly ordered pores of AAO induced the plasmon effect, which affects the efficiency of the BHJ IOSCs. Figure 1d is a cross-sectional FE-SEM image of the ZnO nanotube structure that was formed onto the Au NP-dispersed walls in the AAO pores. The diameter and height of the nanotube could be easily tuned by controlling the pore size and depth of the AAO template. ZnO nanotubes were prepared in the pore wall of the AAO template by spin-coating ZnO at 4000 rpm for 20 s. Subsequently, the sample was maintained in vacuum conditions for 30 min and then thermally heated at 150 °C for 30 min.

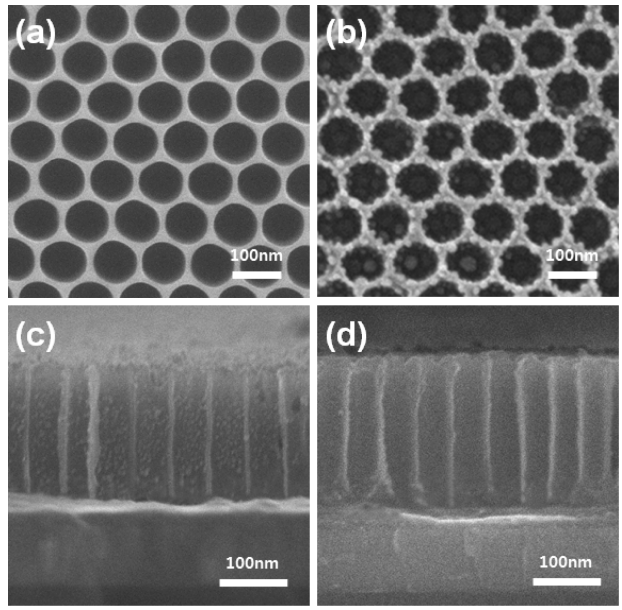

Figure 1. (a and b) FE-SEM images of the AAO template and self-assembled hexagonally well-dispersed Au NPs on the surface and in the pores of AAO. (c) Cross-sectional FE-SEM image of self-assembled well-dispersed Au NPs in the walls of highly ordered pores of the AAO template transferred onto a ZnO/ITO/glass substrate for the fabrication of BHJ IOSCs. (d) Cross-sectional FE-SEM image of ZnO nanotubes on the Au NP-dispersed walls in the AAO pores.

To investigate the near-field induced by Au NPs experimentally, we measured the Raman scattering of rhodamine 6G (R6G) in an AAO template with and without Au NPs (Figure 2). To obtain the Raman signals, 10 mM and 1 μM R6G were utilized. The enhanced intensity of the Raman peaks observed from R6G confirmed the strong electromagnetic field associated with this Au NP array, which enhanced the magnitude of the R6G peaks and demonstrated

dx.doi.org/10.1021/am4045585 | ACS Appl. Mater. Interfaces 2014, 6, 1030−1035

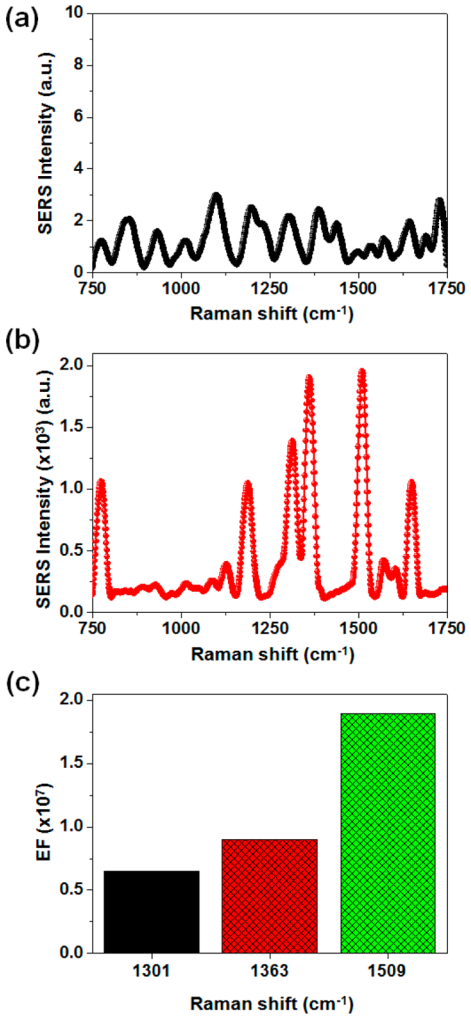

Figure 2. Raman scattering of R6G using the AAO template (a) without and (b) with Au NPs. (c) EFs of the SERS peaks.

the potential for application of this Au NP array to an ultrasensitive SERS substrate. On the basis of the measured results, the analytical enhancement factor (EF) at each main peak was calculated from the equation EF = (I_{SERS}/I_{Raman})-(C_{Raman}/C_{SERS}),[25] where I and C represent the intensity and concentration, respectively. EF of the SERS substrate at a wavenumber of 1509 cm^{-1} was 1.9×10^7 (see Figure 2c for the SERS EFs at other main peaks). Consequently, the AAO template with Au NPs had a stronger Raman scattering than the one without Au NPs. The Raman scattering intensity is proportional to the electric field intensity: a stronger Raman scattering from the structure represents a stronger electric field, which was induced by introducing Au NPs into AAO. When the laser illuminated the Au NPs, a strong local electric field was induced by surface plasmon resonance, and Raman scattering was enhanced by the active-layer-capped Au NPs. These results indicate that a strong near-field is actually induced by introducing Au NPs into AAO, which is consistent with the simulated results that will be discussed further.

We used this Au NP array with AAO to demonstrate a new architecture of plasmon excitation in BHJ IOSCs. Figure 3a–d is a schematic illustration of the preparation of a BHJ IOSC of P3HT:PCBM with Au NPs in the pores of the AAO template. First, a very thin functional ZnO layer was deposited using a sol–gel method on an ITO/glass substrate and thermally

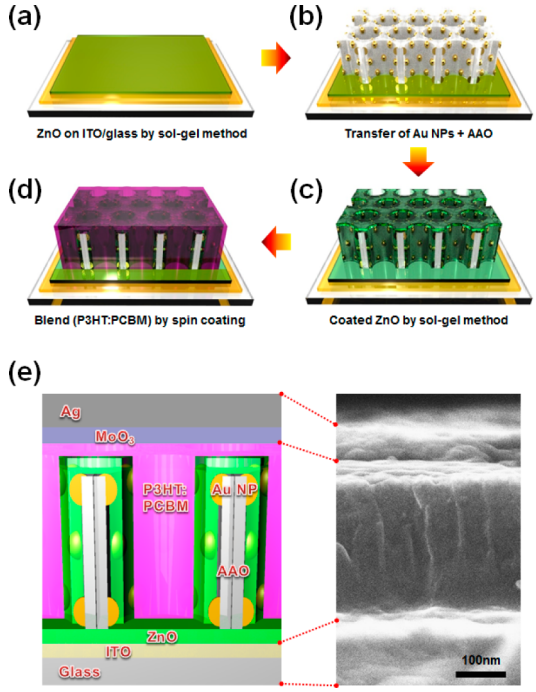

Figure 3. (a–d) Fabrication process of plasmonic IOSC. (e) Schematic and cross-sectional image of fabricated IOSCs with Au NPs.

annealed (Figure 3a). ZnO is a promising candidate for electron collection and as a transport layer in a BHJ polymer solar cell because of its high electron mobility and high transparency in the visible wavelength range. This thin ZnO layer can also be useful for enhancing the adhesion between AAO and the substrate. Second, a free-standing AAO template with Au NPs was carefully transferred onto the ZnO-coated ITO/glass substrate. Then, the sample was annealed at 120 °C to ensure better contact between AAO and the substrate through favorable interaction between AAO and the ZnO thin film of the substrate (Figure 3b). Next, ZnO nanotubes were synthesized in the pores of the AAO template by spin coating of ZnO, as described before in Figure 1d (Figure 3c). Finally, we prepared a P3HT:PCBM blended solution for active-layer deposition by spin coating. Subsequently, this sample was kept in a vacuum and annealed. This process formed P3HT:PCBM blended BHJ polymer nanorods in the prepared ZnO nanotubes with the Au NP array (Figure 3d). Figure 3e represents the schematic illustration and cross-sectional image of a fabricated IOSC. It is found that the P3HT:PCBM blend completely filled in the pores of the AAO template. Hereafter, this structure will be called "NPs_AAO" (the structure without a NP will be called "w/o NPs_AAO"). Further, a MoO_3 layer of 20 nm as the hole conducting layer and a 100-nm-thick Ag layer were deposited to fabricate IOSCs.

Recent studies[26−34] have shown that IOSC devices with metal NPs incorporated in the photoactive region have enhanced light absorption and higher photocurrent. However, the power conversion efficiency (PCE) in these cases might be restricted by exciton quenching with nonradiative energy transfer and the differences between the electronic properties of the metal NPs and conjugated molecules. In contrast, this undesirable quenching does not occur in interfacial metallic nanostructures between ZnO and ITO substrates. In our proposed new architecture of plasmon excitation in BHJ polymer solar cells, the interfacial contact area between the Au

NPs and the active layer is larger than that of conventional BHJ polymer solar cells of horizontal layer-by-layer structure.

It was found that the optical response of the P3HT:PCBM blended nanorods in ZnO nanotubes with Au NP arrays was enhanced by the strong plasmonic field associated with the well-dispersed Au NP array compared to that of the P3HT:PCBM blended nanorods in ZnO nanotubes without the Au NP arrays. Figure 4a shows diffuse-reflectance spectra of

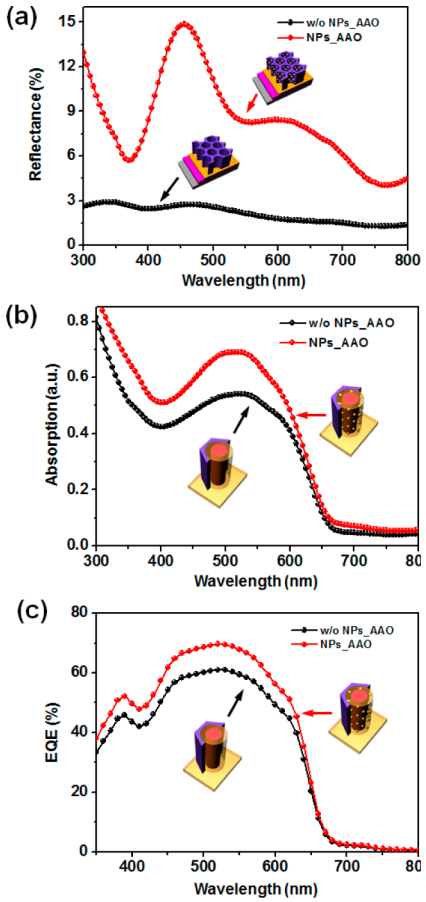

Figure 4. (a) Reflectance spectra of the AAO template without and with AuNPs. (b) Absorption spectra of P3HT: PCBM nanorods in ZnO nanotubes with and without Au NPs. (c) IPCE spectra for two kinds of IOSCs: a reference cell and a plasmonic nanostructure-incorporated cell.

the AAO template with and without Au NPs on ZnO/ITO/glass that are presented to show the influence of Au NPs on the light-scattering effect. The AAO template with Au NPs shows higher lift in the reflectance curve compared to the bare AAO Au NPs. Figure 4b shows the absorption spectra of the P3HT:PCBM nanorods in ZnO nanotubes with and without Au NPs, respectively. Because the plasmon region of Au NPs matches the absorption spectrum of P3HT:PCBM, the absorbance of P3HT:PCBM with Au NPs increases. As a result, the weaker P3HT:PCBM absorbance in the plasmon region is overwhelmed by the stronger plasmon excitation, which results in a profile similar to the surface plasmon band shapes. The absorption of the P3HT:PCBM blended nanorods in ZnO nanotubes with Au NPs in the region from 450 to 650 nm were enhanced significantly.

To clarify the optical response further and the influence of the NPs on the photovoltaic performance, the incident photon-to-current conversion efficiency (IPCE) spectra of the IOSCs containing the NPs_AAO and w/o NPs_AAO structures were obtained, as shown in Figure 4c. The EQE values of the IOSC with Au NPs are improved in comparison to that without NPs in a wide wavelength range, which is also consistent with the reflectance and absorption spectra in parts a and b of Figure 4, respectively. These improvements in the IPCE result from Au NPs, particularly from the efficient electric field associated with plasmon and light scattering. The increased J_{SC} that will be shown in Figure 5d implies that more light is harvested in the active layer because of the efficient plasmonic field and multiple light scattering by Au NPs.

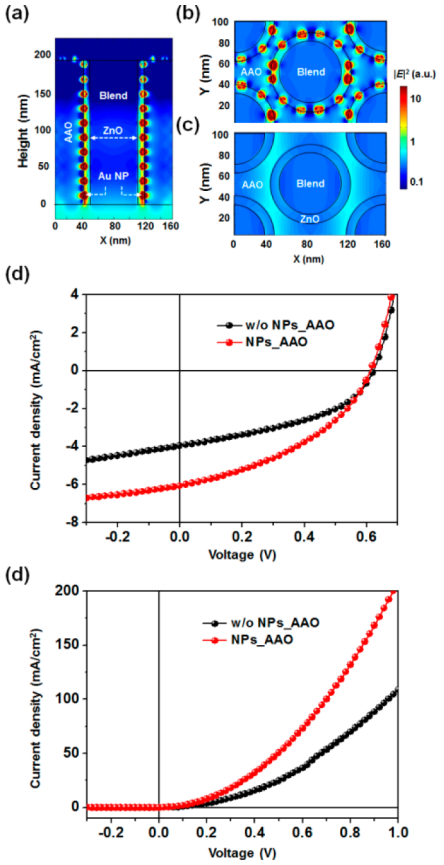

Figure 5. (a) Cross-sectional electric field intensity, $|E|^2$, distribution in IOSC with Au NPs at a wavelength of 548 nm. Plane-view distributions in the cells (b) with and (c) without Au NPs. $J-V$ characteristics of plasmonic IOSCs (d) under AM 1.5 G illumination and (e) in the dark.

Parts a–c of Figure 5 show the electric field distributions in the IOSCs with and without NPs at λ = 548 nm, where the difference in the absorption capacity of the two samples is the largest (Figure 4b). The field enhancement around the NPs clearly indicates excitation of LSPR. A remarkable difference in the distribution of the electric field between the two samples is also seen. The LSPR-enhanced light absorption (Figure 4b) seems to result from three major factors. First, excitation of LSPR resulted in the local enhancement of the electromagnetic field in the vicinity of Au NPs.[35] Therefore, the total number of excitons created in the active layer can be increased. Second, the charge-transfer process of plasmonically excited electrons from Au NPs to ZnO can achieve trap filling in the ZnO layer, reducing the extraction barrier, resistance, and charge

dx.doi.org/10.1021/am4045585 | ACS Appl. Mater. Interfaces 2014, 6, 1030–1035

Table 1. Performance Details (V_{OC}, J_{SC}, FF, and PCE) of the Plasmonic IOSC

	J_{SC} (mA cm^{-2})	V_{OC} (V)	FF	PCE (%)
w/o NPs_AAO	3.98 (±0.32)	0.61 (±0.01)	0.43 (±0.01)	1.07 (±0.21)
NPs_AAO	6.05 (±0.51)	0.61 (±0.02)	0.51 (±0.02)	1.51 (±0.33)

recombination, which enhance electron extraction.[36] Last, light scattering by the NPs lengthens the optical path in the blend layer,[34] thereby enhancing the degree of light absorption. Light scattering, which is beneficial for trapping light in thin absorber materials, becomes more dominant when larger NPs are used.

Spherical Au NPs in air have LSPR at λ = 500 nm. The Au NPs in our samples are hemispherical and have a large contact area with the AAO template. Such a geometry and the underlying layer affect the depolarization field and vary the LSPR peak position. In addition, the ZnO layer capping our Au NPs should lead to significant interaction between the oscillating free electrons in the NPs and the charge carriers in the ZnO layer, which can further alter the spectral characteristics of LSPR. For these reasons, numerical approaches rather than analytical solutions are helpful in understanding our experimental results. Local hot spots at the NP surface and the large field in the NPs are shown in parts a (cross-sectional view) and b (top-view) of Figure 5, and they suggest that each NP concentrates the incoming light into a strongly localized field, enhancing the absorption and scattering cross section of the NP. In the simulation, linearly polarized light along the x axis was considered. Thus, the field between neighboring NPs was larger for the transversely coupled pairs (i.e., along the y axis) than for the longitudinally coupled pairs (i.e., along the x axis).

Figure 5d displays the $J-V$ characteristics, measured under an air mass of 1.5 and global full-sun (AM 1.5G) illumination of 100 mW cm^{-2}, of the two kinds of IOSC devices. The IOSC device without Au NPs has an open-circuit voltage (V_{OC}) of 0.61 V, a J_{SC} of 3.98 mA cm^{-2}, and a fill factor (FF) of 43.2%, as summarized in Table 1. The estimated PCE is as small as 1.07%. In the case of the IOSC with Au NPs, J_{SC} is 6.05 mA cm^{-2} and FF is 50.6%. J_{SC} increases after the incorporation of Au NPs, as expected from the optical results and hypothesis. The V_{OC} values of the two devices are almost identical. Consequently, these results conclude that the performance enhancement of the photovoltaic attributes to the combined effect of the efficient plasmonic field and light scattering induced by Au NPs. The series resistance in the forward bias range, extracted from the $J-V$ curves in the dark (Figure 5e) was decreased after the incorporation of Au NPs in the architecture. It is suggested that Au NPs embedded in the ZnO layer lead to a reduced series resistance; as a result, charge collection of plasmonically excited electrons from Au NPs to ZnO is enhanced.[36] Therefore, it can be concluded that enhancement of the FF is due to the improved charge collection by incorporating Au NPs.

CONCLUSIONS

In summary, we investigated strong plasmonic field generation using a self-assembled hexagonally well-dispersed Au NP array. Using the Au NP array with AAO, we demonstrated a new architecture of plasmon excitation in BHJ IOSCs to enhance the plasmon effect. This architecture increases the interfacial contact between Au NPs and the active layer of the organic solar cell. Light absorption and exciton extraction in the BHJ IOSC increase significantly by the LSPR-induced local field enhancement and the increase in the interfacial contact between Au NPs and the active layer. The improved J_{SC} from 3.975 to 6.050 mA cm^{-2} and the increased PCE from 1.07% to 1.51% by incorporation of the Au NP array suggest that this new architecture enhances the optical response of the BHJ active layer such as the plasmonic field and light scattering. We believe that the results obtained in this study may lead to the realization of higher-efficiency IOSC devices and that this approach will open new areas of study on various plasmon-based phenomena such as the modulation of exciton-plasmon interactions and fluorescence enhancement.

AUTHOR INFORMATION

Corresponding Author

*E-mail: kimsw1@skku.edu. Tel: +82-31-290-7352. Fax: +82-31-290-7410.

Author Contributions

§These authors contributed equally to this work.

Notes

The authors declare no competing financial interest.

ACKNOWLEDGMENTS

This research was supported by National Research Foundation of Korea (NRF) grants funded by the Ministry of Science, ICT & Future Planning (Grants 2012R1A2A1A01002787 and 2009-0083540) and the Energy International Collaboration Research & Development Program of the Korea Institute of Energy Technology Evaluation and Planning funded by the Ministry of Knowledge Economy (Grant 2011-8520010050).

REFERENCES

(1) Kelly, K. L.; Coronado, E.; Zhao, L. L.; Schatz, G. C. *J. Phys. Chem. B* **2003**, *10*, 668−677.
(2) Lal, S.; Link, S.; Halas, N. J. *Nat. Photonics* **2007**, *1*, 641−648.
(3) Lu, L.; Xu, T.; Chen, W.; Lee, J. M.; Luo, Z.; Jung, I. H.; Park, H. I.; Kim, S. O.; Yu, L. *Nano Lett.* **2013**, *13*, 2365−2369.
(4) Lee, J. M.; Kwon, B.-H.; Park, H. I.; Kim, H.; Kim, M. G.; Park, J. S.; Kim, E. S.; Yoo, S.; Jeon, D. Y.; Kim, S. O. *Adv. Mater.* **2013**, *25*, 2011−2017.
(5) Lee, J. M.; Park, J. S.; Lee, S. H.; Kim, H.; Yoo, S.; Kim, S. O. *Adv. Mater.* **2011**, *23*, 629−633.
(6) Stewart, M. E.; Anderton, C. R.; Thompson, L. B.; Maria, J.; Gray, S. K.; Rogers, J. A.; Nuzzo, R. G. *Chem. Rev.* **2008**, *108*, 494−521.
(7) Barnes, W. L.; Dereux, A.; Ebbesen, T. W. *Nature* **2003**, *424*, 824−830.
(8) Murphy, C. J.; Sau, T. K.; Gole, A. M.; Orendorff, C. J.; Gao, J.; Gou, L.; Hunyadi, S. E.; Li, T. *J. Phys. Chem. B* **2005**, *109*, 13857−13870.
(9) Henglein, A. *Chem. Rev.* **1989**, *89*, 1861−1873.
(10) Link, S.; El-Sayed, M. A. *J. Phys. Chem. B* **1999**, *103*, 8410−8426.
(11) Pérez-Juste, J.; Pastoriza-Santos, I.; Liz-Marzán, L. M.; Mulvaney, P. *Coord. Chem. Rev.* **2005**, *249*, 1870−1901.
(12) Lyvers, D. P.; Moon, J.-M.; Kildishev, A. V.; Shalaev, V. M.; Wei, A. *ACS Nano* **2008**, *2*, 2569−2576.
(13) Yang, L.; Cai, Q. *Inorg. Chem.* **2006**, *45*, 9616−9616.

(14) Evans, P. R.; Wurtz, G. A.; Atkinson, R.; Hendren, W.; O'Connor, D.; Dickson, W.; Pollard, R. J.; Zayats, A. V. *J. Phys. Chem. C* **2007**, *111*, 12522−12527.
(15) Li, W.; Camargo, P. H. C.; Lu, X.; Xia, Y. *Nano Lett.* **2009**, *9*, 485−490.
(16) Yang, Y.; Matsubara, S.; Xiong, L.; Hayakawa, T. *J. Phys. Chem. C* **2007**, *111*, 9095−9104.
(17) Laurence, T. A.; Braun, G.; Talley, C.; Schwartzberg, A.; Moskovits, M.; Reich, N.; Huser, T. *J. Am. Chem. Soc.* **2009**, *131*, 162−169.
(18) Nie, S.; Emory, S. R. *Science* **1997**, *275*, 1102−1106.
(19) Talley, C. E.; Jackson, J. B.; Oubre, C.; Grady, N. K.; Hollars, C. W.; Lane, S. M.; Huser, T. R.; Nordlander, P.; Halas, N. J. *Nano Lett.* **2005**, *5*, 1569−1574.
(20) Wang, H. H.; Liu, C. Y.; Wu, S. B.; Liu, N. W.; Peng, C. Y.; Chan, T. H.; Hsu, C. F.; Wang, J. K.; Wang, Y. L. *Adv. Mater.* **2006**, *18*, 491−495.
(21) Gu, G. H.; Suh, J. S. *Langmuir* **2008**, *24*, 8934−8938.
(22) Sander, M. S.; Tan, L.-S. *Adv. Funct. Mater.* **2003**, *13*, 393−397.
(23) Hong, S.; Kang, T.; Choi, D.; Choi, Y.; Lee, L. P. *ACS Nano* **2012**, *6*, 5803−5808.
(24) Choi, Y.-Y.; Choi, K.-H.; Lee, H.; Lee, H.; Kang, J.-W.; Kim, H.-K. *Sol. Energy Mater. Sol. Cells* **2011**, *95*, 1615.
(25) Choi, D.; Choi, Y.; Hong, S.; Kang, T.; Lee, L. P. *Small* **2010**, *6*, 1741−1744.
(26) Atwater, H. A.; Polman, A. *Nat. Mater.* **2010**, *9*, 205−213.
(27) Polman, A.; Atwater, H. A. *Nat. Mater.* **2012**, *11*, 174−177.
(28) Wang, D. H.; Kim, D. Y.; Choi, K. W.; Seo, J. H.; Im, S. H.; Park, J. H.; Park, O. O.; Heeger, A. J. *Angew. Chem., Int. Ed.* **2011**, *50*, 5519−5523.
(29) Wang, D. H.; Park, K. H.; Seo, J. H.; Seifter, J.; Jeon, J. H.; Kim, J. K.; Park, J. H.; Park, O. O.; Heeger, A. J. *Adv. Energy Mater.* **2011**, *1*, 766−770.
(30) Li, X.; Choy, W. C. H.; Huo, L.; Xie, F.; Sha, W. E. I.; Ding, B.; Guo, X.; Li, Y.; Hou, J.; You, J.; Yang, Y. *Adv. Mater.* **2012**, *24*, 3046−3052.
(31) You, J.; Li, X.; Xie, F.-X.; Sha, W. E. I.; Kwong, J. H. W.; Li, G.; Choy, W. C. H.; Yang, Y. *Adv. Energy Mater.* **2012**, *2*, 1203−1207.
(32) Kang, M.-G.; Xu, T.; Park, H. J.; Luo, X.; Guo, L. J. *Adv. Mater.* **2010**, *22*, 4378−4383.
(33) Kulkarni, A. P.; Noone, K. M.; Munechika, K.; Guyer, S. R.; Ginger, D. S. *Nano Lett.* **2010**, *10*, 1501−1505.
(34) Wu, J.-L.; Chen, F.-C.; Hsiao, Y.-S.; Chien, F.-C.; Chen, P.; Kuo, C.-H.; Huang, M. H.; Hsu, C.-S. *ACS Nano* **2011**, *5*, 959−967.
(35) Maier, S. A.; Brongersma, M. L.; Kik, P. G.; Atwater, H. A. *Phys. Rev. B: Condens. Matter Mater. Phys.* **2002**, *65*, 193408.
(36) Zhang, D.; Choy, W. C. H.; Xie, F.; Sha, W. E. I.; Li, X.; Ding, B.; Zhang, K.; Huang, F.; Cao, Y. *Adv. Funct. Mater.* **2013**, *23*, 4255−4261.